LAWRENCE
LIVERMORE
NATIONAL
LABORATORY

LLNL-JRNL-403962

Magnetically Controlled Plasma Waveguide For Laser Wakefield Acceleration

D. H. Froula, L. Divol, P. Davis, J. Palastro, P. Michel, V. Leurent, S. H. Glenzer, B. Pollock, G. Tynan

May 16, 2008

Plasma Physics and Controlled Fusion

Disclaimer

Magnetically Controlled Plasma Waveguide For Laser Wakefield Acceleration

D H Froula, L Divol, P Davis‡, J P Palastro, P Michel, V Leurent and S H Glenzer

Lawrence Livermore National Laboratory, P.O. Box 808, Livermore, California 94551

E-mail: froula1@llnl.gov

B Pollock and G Tynan

Department of Mechanical and Aerospace Engineering Jacobs School of Engineering, and The Center for Energy Research UCSD, University of California at San Diego

PACS numbers:

Abstract. An external magnetic field applied to a laser plasma is shown produce a plasma channel at densities relevant to creating GeV monoenergetic electrons through laser wakefield acceleration. Furthermore, the magnetic field also provides a pressure to help shape the channel to match the guiding conditions of an incident laser beam. Measured density channels suitable for guiding relativistic short-pulse laser beams are presented with a minimum density of 5×10^{17} cm^{-3} which corresponds to a linear dephasing length of several centimeters suitable for mulit-GeV electron acceleration. The experimental setup at the Jupiter Laser Facility, Lawrence Livermore National Laboratory, where a 1-ns, 150 J 1054 nm laser will produce a magnetically controlled channel to guide a < 75 fs, 10 J short-pulse laser beam through 5-cm of 5×10^{17} cm^{-3} plasma is presented. Calculations presented show that electrons can be accelerated to 3 GeV with this system. Three-dimensional resistive magneto-hydrodynamic simulations are used to design the laser and plasma parameters and quasi-static kinetic simulations indicate that the channel will guide a 200 TW laser beam over 5-cm.

‡ Currently at: Department of Physics, University of California at Berkeley

1. Introduction

It has been recently demonstrated [1, 2, 3, 4] that plasma waveguides can extend the propagation range of intense laser beams beyond their inherently short Rayleigh length. Several techniques have been employed to guide intense laser beams in order to enhance harmonic generation [5, 6], laser beam power amplification through backward Raman scattering [7], and the electron beam energy achieved through laser wakefield acceleration [8, 9].

Recently, a novel approach was used to produce optical channels in gas targets using a laser beam to deposit energy along its axis producing a temperature gradient that forces plasma from the high-temperature region producing an axial density channel [1]. The energy in the pre-forming beam can be adjusted to optimize the guiding of a second short-pulse high-power beam. In laser wakefield acceleration experiments, this technique was employed to guide a relativistic laser beam over 10 Rayleigh lengths; this produced one of the first monoenergetic electron beams[8], but the pre-forming energy required limits densities to above $\sim 10^{19}$ cm^{-3}.

In this work, we show that the introduction of an external magnetic field allows a channel to be created at significantly lower densities ($< 10^{18}$ cm^{-3}) while the magnitude of the external field provides control of the shape of the density channel. Specifically the magnetic field (1) reduces the heat flux propagating away from the heater beam increasing the plasma pressure in the center of the beam [10]; (2) controls the particle motion through the magnetic field pressure ($\beta = n_e T_e / B^2$). The first condition localizes the energy deposition providing an increased plasma pressure at low densities while the second condition tends to counteract the plasma pressure; the magnitude of the field provides control of the channel shape allowing the channel to be tuned to conditions required to guide a short-pulse laser beam.

Laser wakefield accelerators produce electric fields on the order 10-100 GeV/m [11]. These fields can be used to accelerate electrons and the energy in the electron beam is determined by the acceleration length where the laser intensity is maintained above relativistic intensities and the laser pulse is not overrun by the accelerated electrons. The latter condition is determined by the "dephasing length" (L_d) and is controlled approximately by the plasma density (n_e);

$$L_d = \lambda_e^3 / \lambda_0^2 \propto \frac{1}{n_e^{3/2}}$$

where λ_e is the electron plasma wavelength and λ_0 is the laser wavelength. Acceleration over a dephasing length of a few meters will produce an electron beam energies comparable to conventional accelerators [12]; in order to achieve acceleration over this range, a laser guide must be developed at electron densities in the range of $10^{16} - 10^{18}$ cm^{-3}.

In Sec. 2, the physics and measurements of laser-plasma interactions in the presence of a large external magnetic field are presented. Section 3 shows experimental results

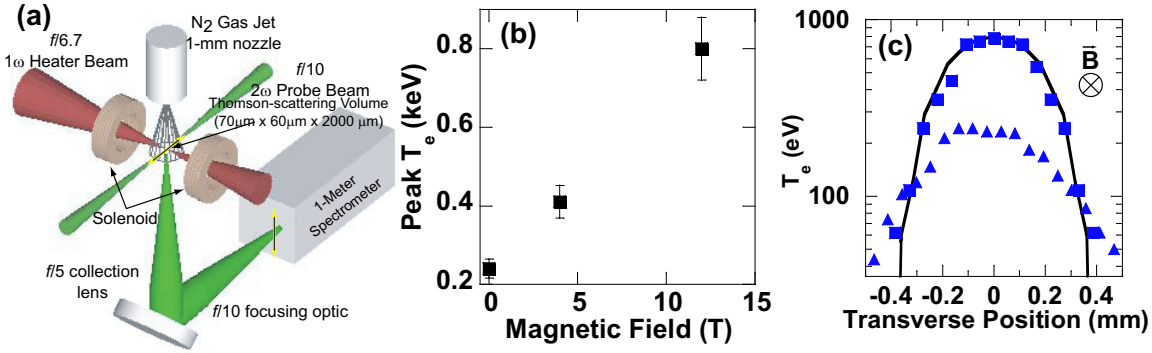

Figure 1. (a) The experimental setup is shown where a high power laser beam interacts with a 1.5-mm gas jet. Both He and N_2 gases were used in the experiments. A solenoid with a 1-cm gap in the middle produces a uniform magnetic filed parallel to the high power beam. A probe beam was aligned perpendicular to the high power beam and used to measure the electron temperature (Thomson scattering) or plasma density (interferometry). (b) The peak electron temperature, at a density of $n_e = 1.5 \times 10^{19}$ cm^{-3}, 1 ns after the rise of the heater beam is measured as a function of magnetic field. (c) The electron temperature profile perpendicular to the heater beam is measured using imaging Thomson scattering and shows a factor of 4 increase in the peak electron temperature when a (squares) B=12 Tesla magnetic field is applied. (triangles) B=0. The solid line is from the hydrodynamic simulations with a magnetic field included.

that demonstrate the ability of the magnetic field to produce a low density channel ($n_e < 1 \times 10^{-18}$ cm^{-3}) suitable for a guiding high power laser. Section 4 presents a platform that will extend the magnetically controlled waveguide over 5-cm and couple a 200 TW short pulse laser beam to accelerate electrons. A 3-dimensional hydrodynamic code that includes magnetic field effects is used to design the conditions to produce a long channel. Quasi-static kinetic simulations demonstrate the ability of this channel to guide a 200 TW short pulse laser beam and accelerate electrons to multi-GeV. Section 5 summarize the current work on producing a magnetically controlled plasma waveguide for GeV wakefield acceleration experiments.

2. Laser Interactions with a Magnetized Plasmas

2.1. Experimental Setup

These experiments were performed in the Jupiter Laser Facility, Lawrence Livermore National Laboratory (Fig. 1(a)). Plasmas were produced in a gas jet with a 1.5 mm diameter cylindrical nozzle and a maximum operating upstream pressure of 10 atm. The opening of the nozzle was aligned 1.5 mm below the target chamber center (TCC). The neutral gas density was well-characterized using interferometery [13]; the peak neutral density used in the experiments discussed here was $n_0 = 8 \times 10^{18}$ cm^{-3}.

A 1ω (1054 nm), 100 J laser beam was focused to a minimum vacuum spot diameter of 150 μm. The laser pulse was 1-ns square. A second laser beam was used as a probe

for either Thomson scattering or interferometry. The probe was 200 ps long and was aligned perpendicular to the high power beam. The time between the beams was varied to study the temporal evolution of the plasma parameters; the relative beam timing was known to 200 ps. For the results discussed here, the probe arrived 1 ns after the rise of the heater beam.

An external magnetic field parallel to the heater beam was generated by a solenoid (modified Bitter magnet [14]). The magnet was driven with a pulsed power system capable of delivering a peak current of 15 kA, resulting in a 12 T field in vacuum at the TCC. The magnetic field was shown to be constant over the laser experiment scale lengths ($\sim$ 1 mm, 1 ns) [15].

2.1.1. Thomson scattering Collective Thomson scattering has been shown to be a valuable diagnostic to measure temporally and spatially resolved density and electron/ion temperatures in laser produced plasmas [16, 17]. In this study, the Thomson scattering probe laser was frequency doubled (2ω) to produce 0.5 J and focused with a 40 cm focal length lens (f/10) to a 70 μm diameter spot. The Thomson-scattered light was collected at an angle of 90°, and collimated by an f/5 lens and imaged with a f/15 focusing lens, on to the 200 μm entrance slit of a 1 meter, 2400 groves/mm, imaging spectrometer. The Thomson-scattering collection system had a magnification of 3. An intensified gated charge coupled device (CCD) with 26 μm square pixels was coupled to the spectrometer providing a spectral resolution of $\delta\lambda = 0.09$ nm and a spatial resolution perpendicular to the high power heater beam better than δx = 30 microns. The Thomson-scattering volume was defined by the beam waist of the probe laser (70 μm diameter) and the projection of the spectrometer slit into the plasma plane.

2.1.2. Interferometry The density profile was measured using a Mach-Zehnder interferometer. The plasma was imaged by a 2.5 inch diameter lens with a 30 cm focal length onto a CCD with 9 micron pixels. The magnification of the system was 5 and had a spatial resolution of 20 microns. For the high density measurements ($n_e = 1.5 \times 10^{19}$ cm^{-3}), the probe beam was frequency doubled ($\lambda = 527$ nm) to reduce the sensitivity of the system (i.e. reduce the number of fringe shifts).

2.2. Effect of an external magnetic field on electron temperature

Imaging collective Thomson scattering was used to measure the electron temperature profile perpendicular to the heater beam and demonstrates the power of an external magnetic field to influence the plasma conditions for the creation of a plasma waveguide. Figure 1(b) shows the measured peak electron temperature as a function of the applied magnetic field. A 12 Tesla magnetic field increases the peak electron temperature by a factor of four by quenching the nonlocal heat transport [10]. At low densities, suppression of the nonlocal heat flux is a prerequisite for channel production.

It is found that a 12 Tesla external magnetic field oriented parallel to a high

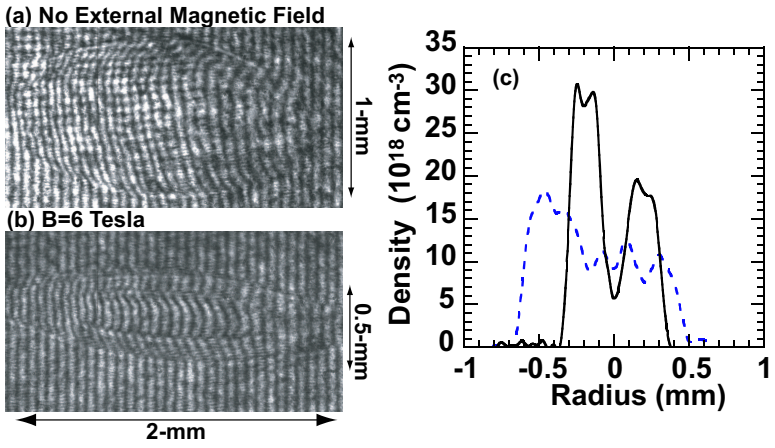

Figure 2. Interferometric images measure the phase change induced by the line averaged plasma density when (a) no magnetic field and (b) a B=6 Tesla external magnetic field is applied. (c) The phase change is Abel inverted to provide a measure of the radial plasma density with (solid curve) and without (dashed curve) an external magnetic field for an initial He neutral density of $n_0 = 8 \times 10^{18}$ cm^{-3}.

power laser beam inhibits electron thermal transport perpendicular to the heater beam, reducing the heat flux by a factor of $\kappa_\perp/\kappa_\parallel = 0.7$ where $\kappa_\parallel, \kappa_\perp$ are the conductivities parallel and perpendicular to the magnetic field respectively. In these experiments, the magnetic field serves to restrict the electron thermal conduction losses, but for the high density ($n_e = 1.5 \times 10^{19}$ cm^{-3}), high magnetic field (B=12T) conditions, the field is not sufficient to confine the hot plasma to the laser-heated core ($\beta \simeq 20$).

Figure 1(c) shows the spatial profile of the heat wave for the highest magnetic field experiments (B=12 T). These results are compared with simulations using a hydrodynamic code that solves the classical heat transport equations originally presented by Braginskii [18]. These simulations use the electron heat flux determined by the minimum between the Braginskii heat flux (q_B) and the free-streaming heat flux ($q_{fs} = n_e T_e v_e$);

$$\mathbf{q}_B = -\kappa_\parallel \nabla_\parallel T_e - \kappa_\perp \nabla_\perp T_e \tag{1}$$

where the cross-thermal conductivities have been neglected due to the axisymmetry of the experiment and the conductivities can be approximated for the high magnetic field simulations by [19, 20],

$$\kappa_\parallel = 3.2 \frac{Z n_e T_e \tau_{ei}}{m_e};$$

$$\kappa_\perp = 4.7 \frac{Z n_e T_e \tau_{ei}}{m_e \omega_{ce}^2 \tau_{ei}^2};$$

Comparing the conductivity effected by the external magnetic field ($\kappa_\perp$) with the conductivity that is not effected by the external magnetic field ($\kappa_\parallel$) provides an estimate of the reduction in heat flux for a 10 T magnetic field, $\kappa_\perp/\kappa_\parallel = 0.7$.

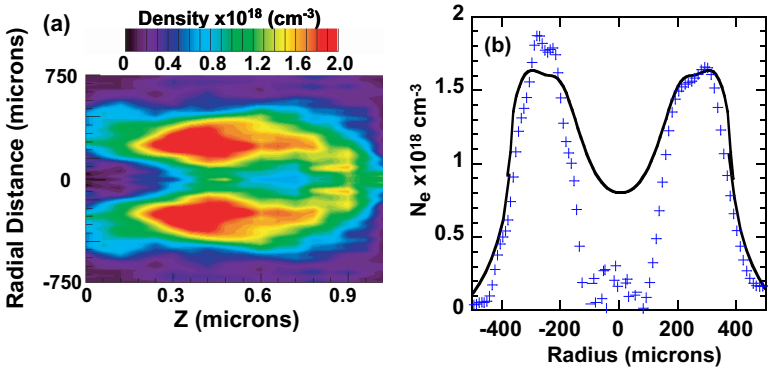

Figure 3. (a) A 2-dimensional Abel inverted density profile measured at an initial neutral He density of $n_0 = 7.5 \times 10^{17}$ cm^{-3} shows a 1-mm long channel. The heater beam propagates from left to right. (b) The measured density profile (symbols) taken from the center (z=0.5 mm) of the channel is shown. (black curve) The electron density is calculated for the conditions of the measurement.

2.3. Effect of an external magnetic field on density

Figure 2 shows a factor of two reduction in the extent of the plasma when a 6 Tesla magnetic filed is applied. Furthermore, this reduction in expansion leads to a density channel and is a direct result of the increased on-axis electron temperature (see Sec. 2.2). The increased electron temperature produces a large pressure driving plasma from the center of the laser beam.

When no magnetic field is applied, Abel inverting the interferograms shows no evidence of a channel and a central density of $n_e = 1.5 \times 10^{19}$ cm^{-3}. When a 6 Tesla magnetic field is applied, the hot plasma is pushed against the cold plasma-gas interface compressing the density along the outer shell to a factor of ~ 1.5 above the background density. The asymmetry in the profiles is a result of the neutral density gradient produced by the gas jet.

Initially the simulations show a background magnetic field throughout the plasma. At 1.5 ns, the field at the center of the plasma drops from the vacuum field of 12 T to 6 T, while the field at the heat front is compressed to nearly 16 T. The magnetic field compression closely follows the radial density compression due to the expanding plasma; initially, the magnetic field is trapped in the plasma, but as the temperature gradient resulting from the local laser beam heating creates a pressure gradient lowering the density in the center of the plasma, the field is pulled out by plasma expansion and compressed at the heat front. The evolution of the magnetic field can be derived from Ohm's law. The magnetic field convects with the flow and diffuses due to joule heating;

$$\frac{\partial \mathrm{B}_z}{\partial t} - \nabla \cdot (\mathbf{v}\mathrm{B}_z) = \frac{\eta}{\mu_o}\nabla^2\mathbf{B} \tag{2}$$

where $\eta_\perp \sim 1 \times 10^{-4} Z \ln(\Lambda)/T_{eV}^{3/2}$ is the plasma resistivity and $\ln(\Lambda) \sim 8$ is the Coulomb logarithm. Equation 2 shows that when the plasma resistivity is small (i.e. perfect

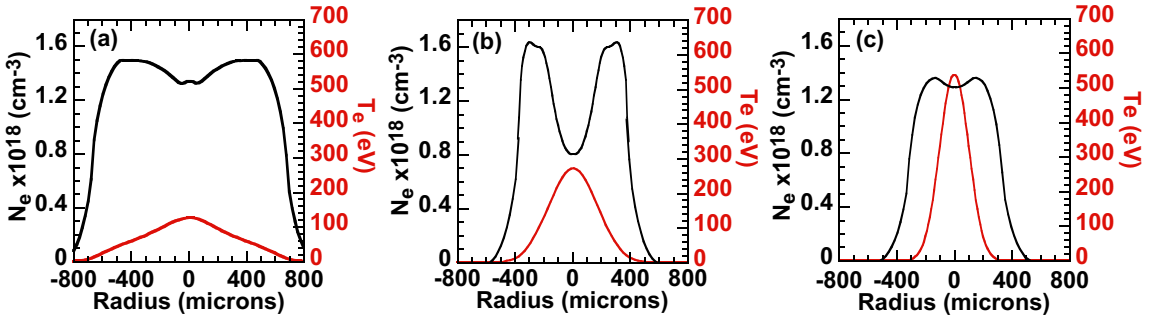

Figure 4. Hydrodynamic simulations that implement Braginskii heat transport demonstrate the effects of a magnetic field on the channel formation at a low initial He neutral density ($n_0 = 7.5 \times 10^{17}$ cm^{-3}); (a) When no magenetic field is used (B=0), the electron temperature is broad and no channel is produced. (b) A magnetic field of B=3 Tesla, increases the electron temperature inside of the laser beam by a factor of 3 and produces a channel with a minimum density of $n_e = 8 \times 10^{17}$ cm^{-3}. (c) Increasing the magnetic field to 30 Tesla continues to increase the electron temperature, but the magnetic field pressure balances the plasma pressure and no channel is produced.

conductor), magnetic field transport by convection greatly exceeds transport by diffusion and the magnetic field will be frozen into the expansion so that [21],

$$\frac{n_e(\mathrm{t})}{n_e(\mathrm{t{=}0})} \sim \frac{\mathrm{B(t)}}{\mathrm{B(t{=}0)}}. \tag{3}$$

3. A plasma waveguide at low densities

Optical channels are produced in gas targets by creating a temperature gradient using a laser beam to pre-form a plasma where the energy in the beam is adjusted to optimize the guiding of a short-pulse high-power beam over 10 Rayleigh lengths, but the energy required to form a channel limits densities to above $\sim 10^{19}$ cm^{-3} [1]. Figure 2(c) reproduces the fact that when no magnetic field is employed at a density of $n_e = 1.5 \times 10^{19}$ cm^{-3} no channel is produced. The introduction of an external magnetic field allows a channel to be created at significantly lower densities ($< 10^{18}$ cm^{-3}) while the field produces a pressure that is used to counteract the plasma pressure and the magnitude of the field provides control of the channel shape allowing the channel to be tuned to conditions required to guide a short-pulse laser beam.

Figure 3 shows a 1-mm long channel with a minimum electron density less than $n_e < 1 \times 10^{18}$ cm^{-3}. A 3 Tesla external magnetic field, 100 J pre-forming laser beam, and initial He neutral density of $n_0 = 7.5 \times 10^{17}$ cm^{-3} was used to produce this channel. Figure 3(b) compares the measured density channel with the hydrodynamic simulations.

Figure 4 demonstrates the ability of the magnetic field to control the minimum plasma density; when no magnetic field is applied, the on axis density is equivalent to the background density; no channel is produced. The peak electron temperature is 100 eV and the details of the temperature gradient are dependent on nonlocal physics [22]. Increasing the magnetic field such that the heat flux is reduced, increases the peak

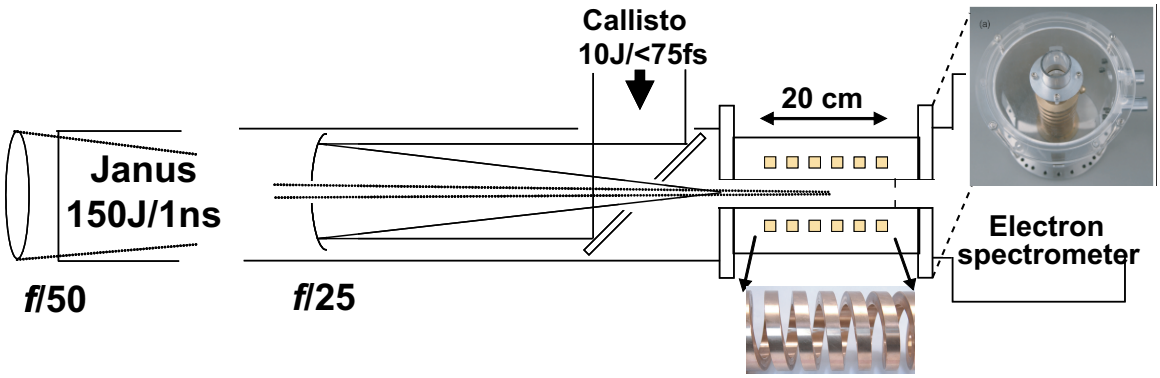

Figure 5. A schematic of an laser wakefield accelerator designed to produce GeV electrons is shown. A 1-ns long, 150 J laser beam is used to produce a multi-centimeter magnetically controlled optical plasma waveguide. A 150 TW short pulse laser is focused at the entrance of the waveguide.

electron temperature by a factor of 3. The particles are not confined by the magnetic filed ($\beta > 1$) and the centrally heated electrons move radially away from the laser beam producing the density channel shown in Fig. 4(b). When the magnetic field is increased further, the electron temperature continues to increase, but the particles are confined ($\beta > 1$) and no channel is produced [Fig. 4(c)].

4. Multi-Centimeter Laser Wakefield Accelerator

Laser wakefield acceleration employs a high-intensity laser beam to separate the charge in a plasma producing electric field gradients 1000 times larger than conventional accelerators. Injecting electrons into this field has produced monoenergetic electron beams [23, 8, 24, 9]; the energy in this beam is determined by the length in which the short pulse laser remains above relativistic intensities and the electrons do not out run the wake which travels at the group velocity of the laser beam. The former condition requires an optical channel while the latter condition requires low densities. The magnetically controlled optical plasma waveguide provides a guiding structure at the densities required to produce greater than 10 GeV monoenergetic electron beams [12].

4.1. Experimental Setup

Figure 5 shows our plan for a laser wakefield accelerator using an extended magnetically controlled plasma channel to guide a 200 TW short pulse laser. To expand the plasma waveguide beyond the 1-mm experiments discussed in Sec. 3, each system is lengthened; the solenoid, gas-target, and Rayleigh length are extended to produce a platform that will generate a $>$ 5-cm long channel at densities less than $n_e < 1 \times 10^{18}$ cm^{-3}.

4.1.1. Laser Configuration The long-pulse Janus Laser and the short-pulse Callisto Laser are currently being directed into a common target chamber at the Jupiter Laser

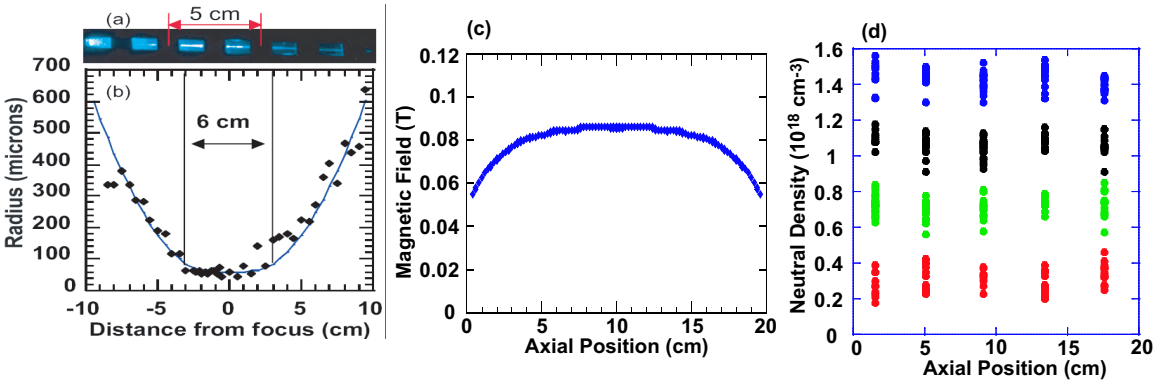

Figure 6. (a) Emission from a plasma column generated with a 3 Tesla magetnic field and 100 J is shown. (b) The radius of the f/50 long-pulse beam is less than 100μm over 6 cm. (c) The measured axial magnetic field profile of the solenoid is measured to be uniform over 12 cm; the maximum field for this system is 4 Tesla. (d) The neutral gas density along the axis of the solenoid is measured for several backing pressures (blue) 800 psi, (black) 600 psi, (green) 400 psi, (red) 200 psi.

Facility, Lawrence Livermore National Laboratory. The long-pulse laser will be used to produce the waveguide delivering 150 J of 1054 nm laser light in a 1-ns long square pulse. The Callisto laser system has recently been upgraded to produce $<$ 75 fs long, 10 J laser pulses. This 150 TW ultra-short pulse laser system coupled with the long pulse capabilities of Janus provides a unique and powerful platform for wakefield acceleration.

Figure 6(b) shows the vacuum intensity for the long-pulse laser beam when an f/50 lens is used to extend the Raleigh length. The minimum laser spot is measured to be a few times diffraction limited ($\sigma = 75$ microns) and the radius remains below 100 microns over 6 cm.

4.1.2. Solenoid An electromagnetic solenoid was designed as part of a low-inductance circuit to provide long, uniform magnetic fields for optical waveguide production. Beginning with a solid block of phosphorus bronze, the solenoid shown in Fig. 6, was machined to be 20 cm long and have 8 turns with a bore diameter of 5.1 cm. The current that generates the magnetic field is supplied by a pulsed power system capable of storing 28.8 kJ and driving nearly 100 kA through the magnetic [15]. This system is capable of delivering a 4 Tesla uniform field over 12 cm [Fig. 6(c)] [25].

4.1.3. Gas Tube A 3/4 inch tube is aligned down the center of the solenoid to isolate the neutral gas from the high voltage. Figure 6(d) shows the measured neutral gas density produced along the axis of the tube. The density in the gas tube was characterized using a time resolved interferometer. A 4-mm aperture is used on the upstream side of the tube to maintain the uniform density (Fig. 5).

Figure 6(a) shows initial experiments that demonstrate a 5-cm long plasma column. The image is recorded by a gated charge-coupled device (CCD) that time averages the visible plasma emission (400-800 nm) for 20 ns. Future experiments will incorporate

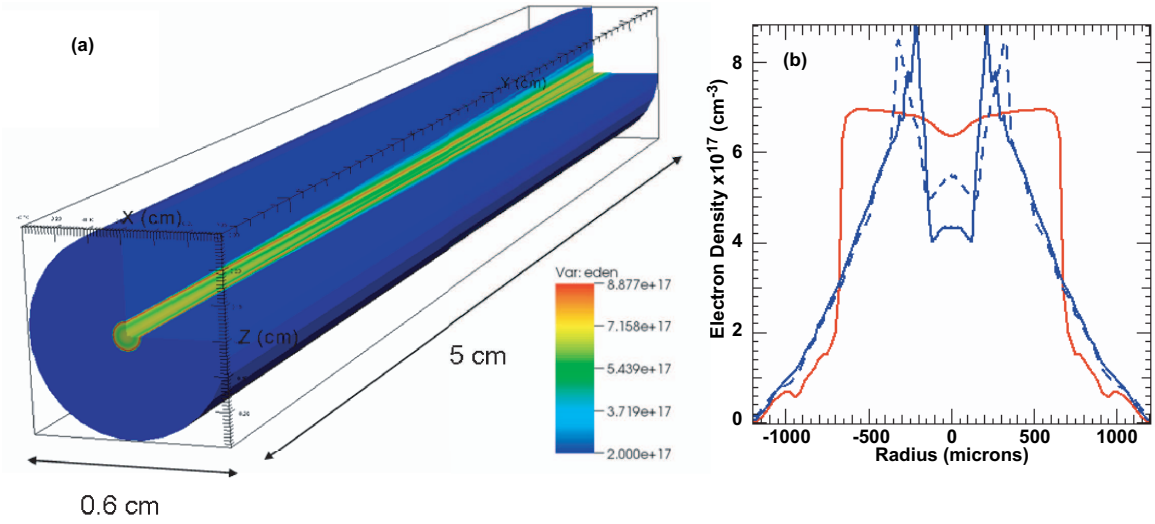

Figure 7. (a)Three-dimensional hydrodynamic simulations are used to demonstrate a 5-cm-long channel at densities required to accelerate electrons to multiple GeV.(b) The transverse electron density at best focus is shown with a flux limiter of $f = 1$ (red), $f = 0.05$ (dashed) and $f = 0.01$ (blue) at the end of the 1 ns laser pulse. A 2 Tesla external magnetic field corresponds to an effective flux limiter of $f = 0.005 - 0.02$ and allows the creation of a waveguide in a low density plasmas over multi-centimeters.

interferometry and Thomson scattering to measure the plasma density and temperature profiles. This experimental set-up will then serve as a platform for LWFA experiments with a 150TW short-pulse laser.

4.2. Simulations

4.2.1. 3D Hydrodynamics In order to assess the feasibility of a 5-cm-long channel at low densities ($< 10^{18}$ cm^{-3}), we have performed hydrodynamics simulations with the code HYDRA [26]. While HYDRA includes an MHD package, it is not currently coupled to the heat conduction models, therefore, the heat flux was limited using a flux limiter calculated to match the effective limit produced by the external magnetic field ($\kappa_\perp/\kappa_\parallel$).

Figure 7(a) shows results of simulations that approximate the reduced transverse heat transport for a 2 Tesla external magnetic field and conditions produced by our current system (See Sec. 4). Running the same simulation without an external magnetic field (i.e. no flux limiter) leads to an electron density bump along the laser propagation axis as transverse heat conduction quickly diffuses strong density perturbations (Fig. 7(b)).

These simulations use a constant background helium neutral density of 3.75×10^{17} cm^{-3}, a laser energy of 100 J over 1 nanosecond and a focal spot of 150μm FWHM with an $f/50$ lens. Figure 7(b) shows results for two simulations where a flux limiter of $f = 0.01$ and $f = 0.05$ were used. Both show qualitatively similar channels with a width between 200 and 400 μm FWHM, a central electron density of 5×10^{17} cm^{-3}, and a peak density of 10^{18} cm^{-3}. The electron temperature varied between 50 and 150 eV.

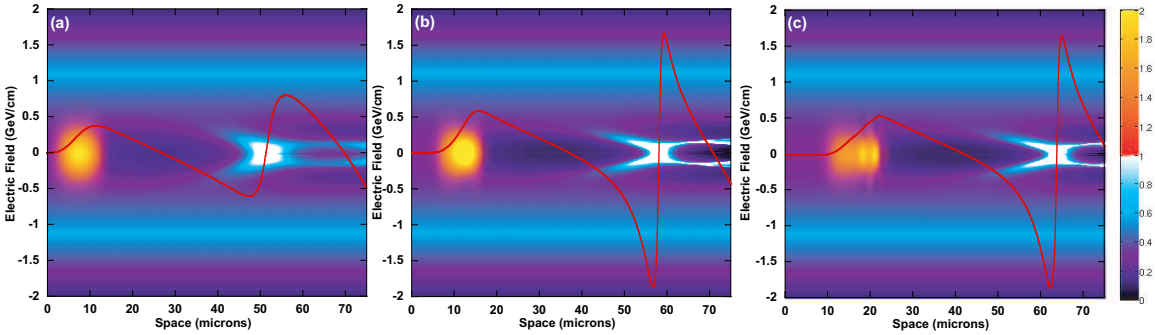

Figure 8. Electron density contours (blue scale) showing the presence of the channel and the evolution of the wake field are shown as the short pulse beam (red scale) propagates from the (a) entrance of the channel (0 cm), (b) midway through the channel (2.5 cm), and (c) at the end of the channel (5 cm). The electric filed generated by the axial wake field is plotted (red curve; left axis).

For these parameters the magnetic field has a large effect on the plasma; the electron cyclotron frequency (ω_{ce}) is much larger than the collision rate (τ_{ei}) $\omega_{ce}\tau_{ei} \approx 5 - 15$ and the heat flux is significantly reduced ($\kappa_\perp/\kappa_\parallel \approx 0.002 - 0.02$) [19]. It should be noted that recent work [27] suggests that this simple estimate of the transverse thermal conductivity when an external B-field is applied could become inaccurate as the spatial evolution of the magnetic field over nanosecond time scales can be quite complicated, with both advection and the Nernst effect competing.

From these simulations, we conclude that a relatively low external magnetic field (1-3 T) is enough to tailor a laser-guiding channel at the densities required for laser wakefield acceleration over multiple centimeters. We are planning to improve our modeling capabilities by coupling the heat transport modeling to the B-field evolution in the near future.

4.2.2. High Power Laser Guiding We simulate the interaction of the short-pulse laser with the background plasma channel using WAKE [28]. Propagation of both a 100 and 200 TW, 50 fs FWHM laser pulse was simulated in a parabolic leaky plasma channel and a uniform plasma over 5 cm. The parameters for the channel were given by the HYDRA simulations where a 2 Tesla magnetic field was applied to produce the channel (See Fig. 7(b)).

Figure 8 shows a 200 TW laser pulse propagating through the 5-cm long channel. The wakefield is strongly driven evident in the large piling of charge one plasma period behind the pulse. In addition, the effect of dispersion on the group velocity of the laser beam is discernable as the pulse begins to split [29]. The short pulse laser used an initial matched channel spot size of 70 microns FWHM.

WAKE assumes a low background plasma density ($\omega_p << \omega_0$), allowing for separation of the electron response into a high frequency and ponderomotive component. In addition, the evolution of the laser envelope is assumed to be slow compared to transit time of electrons through the pulse. As a result, upon averaging over the rapid laser

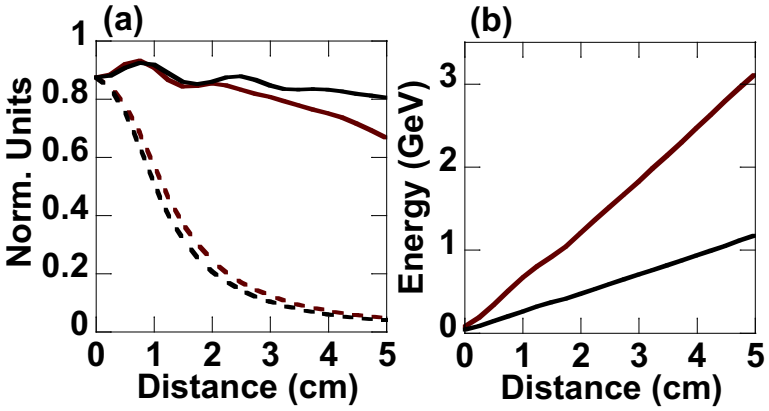

Figure 9. (a) The normalized short pulse energy in one radial sigma is plotted as a function of distance for the 100 TW (black) and 200 TW (red) cases. When a channel is employed (solid) there is significantly less diffraction than when a channel is not used (dotted). (b) The electron energy gain as a function of distance for an electron entering at the beginning of the channel for the 100 TW (black) and 200 TW (red) simulations.

induced oscillations, the motion of the plasma is solely a function of the wave frame coordinate (z-ct). We note that for the channels and pulses considered here $\omega_p/\omega_0 << 1$, and $\Delta t\omega_p << \omega_0/\omega_p$ where Δt is the FWHM of the laser pulse; both assumptions are well justified. WAKE solves an envelope equation for the time evolution of the pulse in one transverse and one longitudinal dimension. Inclusion of group velocity dispersion to lowest order in ω_p/ω_0 allows for longitudinal modifications to the pulse. The pulse is dynamically altered by the presence of the plasma. The laser pulse drives a ponderomotive current in the plasma modifying the background density, which alters the pulse evolution.

Figure 9(a) shows the laser energy contained within the wave guide by averaging over one transverse sigma normalized to the total laser energy. For both unguided cases, the pulse undergoes rapid diffraction and the 200 TW pulse is slightly self-focused. The plasma channel limits diffraction for both laser powers which is evident in the high one-sigma throughput: 91% and 77% for the 100 TW and 200 TW respectively. The 200 TW pulse drives a stronger wake, transferring more of its energy to the plasma, resulting in a smaller throughput than the 100 TW pulse. This high throughput at 5 cm is promising for future plans to scale the length of the guiding structure to > 10 cm.

Figure 9(b) shows the expected energy gain for an electron accelerated by guided 100 and 200 TW laser pulses. We estimate this energy gain by averaging the axial wake field over the accelerating phase, and integrating over the length of the plasma channel. The expected energy gain over 5 cm for the 100 TW and 200 TW pulses is 1 and 3 GeV respectively. This compares well to other studies [12]. Furthermore, this energy gain remains linear in spite of the one-sigma depletion of the laser pulse.

5. Summary

We present a method to extend the propagation range of intense laser beams beyond their inherently short Rayleigh length at densities relevant to accelerating electrons to GeV energies by employing an external magnetic field to a laser produced plasma. An optical plasma waveguide is produced by reducing the heat flux propagating from a laser beam using an external magnetic field. Thomson-scattering measurements show a factor of 3 increase in the electron temperature when a magnetic field is applied. This increase in temperature is shown to create a channel at densities less than $n_e < 10^{18}$ cm^{-3}. Furthermore, the magnetic field produces a pressure that can be used to counteract the plasma pressure and the magnitude of the field provides control of the channel shape allowing the channel to be tuned to conditions required to guide a short-pulse laser beam.

A laser wakefield accelerator that implements the magnetically controlled plasma waveguide is presented along with 3-dimensional hydrodynamic simulations that show a 5-cm channel at a density of 5×10^{17} cm^{-3}. Quasi-static kinetic simulations are used to propagate a 200 TW short pulse laser through this channel suggesting that electrons can be accelerated to 3 GeV.

6. Acknowledgements

We would like to thank Professor A. Offenberger for his valuable contributions to the solenoid designs and general discussions on the physics of magnetic fields in laser plasmas. The authors would also like to acknowledge T. Antonsen for use of WAKE. This work was partially supported by LDRD 08-LW-070 and performed under the auspices of the U.S. Department of Energy by Lawrence Livermore National Laboratory under Contract DE-AC52-07NA27344.

7. References

[1] Cgr Geddes, C Toth, J Van Tilborg, E Esarey, Cb Schroeder, J Cary, and Wp Leemans. Guiding of relativistic laser pulses by preformed plasma channels. *Phys. Rev. Lett.*, 95(14):–, 2005.

[2] E. W. Gaul, S. P. Le Blanc, A. R. Rundquist, R. Zgadzaj, H. Langhoff, and M. C. Downer. Production and characterization of a fully ionized he plasma channel. *Applied Physical Letters*, 77(25), 2000.

[3] C. G. Durfee and H. M. Milchberg. Light pipe for high intensity laser pulses. *Phys. Rev. Lett.*, 71:2409–2412, 1993.

[4] A. Butler, D. J. Spence, and S. M. Hooker. Guiding of high-intensity laser pulses with a hydrogen-filled capillary discharge waveguide. *Phys. Rev. Lett.*, 89(185003), 2002.

[5] C. G. Durfee, A. R. Rundquist, S. Backus, C. Herne, M. M. Murnane, and H. C. Kapteyn. Phase matching of high-order harmonics in hollow waveguides. *Phys. Rev. Lett.*, 83:2187–2190, 1999.

[6] A. Rundquist, C. G. Durfee, Z. Chang, C. Herne, S. Backus, M. M. Murnane, and H. C. Kapteyn. Phase-matched generation of coherent soft x-rays. *SCIENCE*, 280(5368):1412–1415, 1998.

[7] Y. Ping, I. Geltner, A. Morozov, N. J. Fisch, and S. Suckewer. Raman amplification of ultrashort laser pulses in microcapillary plasmas. *Physical Review E*, E66(046401), 2002.

[8] Cgr Geddes, C Toth, J Van Tilborg, E Esarey, Cb Schroeder, D Bruhwiler, C Nieter, J Cary, and Wp Leemans. High-quality electron beams from a laser wakefield accelerator using plasma-channel guiding. *NATURE*, 431(7008):538–541, 2004.

[9] W. P. Leemans. Gev electron beams from a centimeter-scale accelerator. *Nature*, 696, 2006.

[10] D. H. Froula, P. F. Davis, B. B. Pollock, L. Divol, J. S. Ross, J. Edwards, R. P. J. Town, D. Price, S. H. Glenzer, A. A. Offenberger, G. R. Tynan, and A. N. James. Quenching of the nonlocal electron heat transport by large external magnetic fields in a laser produced plasma measured with imaging thomson scattering. *Phys. Rev. Lett.*, 98:135001, 2007.

[11] T. Tajima and J. M. Dawson. Laser electron accelerator. *Phys. Rev. Lett.*, 43:267–270, 1979.

[12] W Lu, M Tzoufras, C Joshi, Fs Tsung, Wb Mori, J Vieira, Ra Fonseca, and Lo Silva. Generating multi-gev electron bunches using single stage laser wakefield acceleration in a 3d nonlinear regime. *PHYS REV SPEC TOP-AC*, 10(6):–, 2007.

[13] Dh Froula, P Davis, L Divol, Js Ross, N Meezan, D Price, Sh Glenzer, and C Rousseaux. Measurement of the dispersion of thermal ion-acoustic fluctuations in high-temperature laser plasmas using multiple-wavelength thomson scattering. *Phys. Rev. Lett.*, 95(19):–, 2005.

[14] F. Bitter. *Rev. Sci. Instrum.*, 10:373, 1939.

[15] B. B. Pollock, D. H. Froula, P. F. Davis, J. S. Ross, S. Fulkerson, J. Bower, J. Satariano, D. Price, K. Krushelnick, and S. H. Glenzer. High magnetic field generation for laser-plasma experiments. *Rev. Sci. Instrum.*, 77:114703, 2006.

[16] S. H. Glenzer, W. Rozmus, B. J. Macgowan, K. G. Estabrook, J. S. De Groot, and G. B. Zimmerman. Thomson scattering from high-z laser-produced plasmas. *Phys. Rev. Lett.*, 82(1):97, 1999.

[17] D. H. Froula, L. M. Divol, and S. H. Glenzer. Measurement of nonlinear growth of ion-acoustic waves in two-ion-species plasmas with thomson scattering. *Phys. Rev. Lett.*, 88(10):105003, 2002.

[18] S. I. Braginskii. *Zh. Eksp. Teor. Fiz.*, 33:459, 1957.

[19] E. M. Epperlein and M. G. Haines. Plasma transport coefficients in a magnetic field by direct numerical solution of the fokker-planck equation. *Phys. Fluids*, 29(4):1029–1041, 1986.

[20] J. D. Huba. *NRL Plasma Formulary.* Washington, DC, 2000.

[21] N. H. Burnett and A. A. Offenberger. Magnetohydrodynamic behavior of a laser-heated solenoid. *J. Appl. Phys.*, 45(5):2155, 1974.

[22] G. Gregori, S. H. Glenzer, J. Knight, C. Niemann, D. Price, D. H. Froula, M. J. Edwards, R. P. J. Town, W. Rozmus, A. Brantov, W. Rozmus, and V. Yu. Bychenkov. Effect of nonlocal transport on heat-wave propagation. *Phys. Rev. Lett.*, 92(20):205006, 2004.

[23] J Faure, Y Glinec, A Pukhov, S Kiselev, S Gordienko, E Lefebvre, Jp Rousseau, F Burgy, and V Malka. A laser-plasma accelerator producing monoenergetic electron beams. *NATURE*, 431(7008):541–544, 2004.

[24] Spd Mangles, Cd Murphy, Z Najmudin, Agr Thomas, Jl Collier, Ae Dangor, Ej Divall, Ps Foster, Jg Gallacher, Cj Hooker, Da Jaroszynski, Aj Langley, Wb Mori, Pa Norreys, Fs Tsung, R Viskup, Br Walton, and K Krushelnick. Monoenergetic beams of relativistic electrons from intense laser-plasma interactions. *NATURE*, 431(7008):535–538, 2004.

[25] B. B. Pollock, D. H. Froula, G. R. Tynan, L Divol, D Price, R. Costa, F. Yepiz, S. Fulkerson, F. Mangini, and S. H. Glenzer. *To be published RSI*, 2007.

[26] M. M. Marinak, G. D. Kerbel, N. A. Gentile, O. S. Jones, D. H. Munro, S. Pollaine, T. R. Dittrich, and S. W. Haan. Three-dimensional hydra simulations of national ignition facility targets. *Phys. Plasmas*, 8(5):2275, 2001.

[27] C. P. Ridgers and R. J. Kingham. Magnetic cavitation and the reemergence of nonlocal transport in laser plasmas. *Phys. Rev. Lett.*, 100(075003), 2008.

[28] P. Mora and T. M. Antonsen. Kinetic modeling of intense, short laser pulses propagating in tenuous plasmas. *Phys. Plasmas*, 4(1):217, 1997.

[29] J. Wu and T. M. Antonsen. Laser pulse splitting and trapping in tenuous gases. *Phys. Plasmas*,

10(6):2254, 2003.